


RESEARCH ARTICLE

Resting-state functional magnetic resonance imaging reveals functional connectivity alteration in the experimental autoimmune encephalomyelitis model of multiple sclerosis

Pietro Bontempi¹ | Giusi Piccolantonio¹  | Alice Busato^{2,3} | Anita Conti⁴ | Gabriele Angelini⁵ | Nicola Lopez⁵ | Alessandro Bani⁵ | Gabriela Constantin⁵ | Pasquina Marzola¹

¹Department of Engineering for Innovation Medicine, University of Verona, Verona, Italy

²Department of Computer Science, University of Verona, Verona, Italy

³Evotec Company, Verona, Italy

⁴Department of Diagnostics and Public Health, University of Verona, Verona, Italy

⁵Department of Medicine, University of Verona, Verona, Italy

Correspondence

Pasquina Marzola, Department of Engineering for Innovation Medicine, University of Verona, Verona, Italy.

Email: pasquina.marzola@univr.it

Funding information

This work was supported by Fondazione Italiana Sclerosi Multipla, Grant 2019/PR-Single/034.

Abstract

Multiple sclerosis (MS) is an autoimmune degenerative disease targeting white matter in the central nervous system. The most common animal model that mimics MS is experimental autoimmune encephalomyelitis (EAE) and it plays a crucial role in pharmacological research, from the identification of a therapeutic target to the in vivo validation of efficacy. Magnetic resonance imaging (MRI) is largely used to detect MS lesions, and resting-state functional MRI (rsfMRI) to investigate alterations in the brain functional connectivity (FC). MRI was mainly used in EAE studies to detect lesions in the spinal cord and brain. The current longitudinal MRI study aims to validate rsfMRI as a biomarker of the disease progression in the myelin oligodendrocyte glycoprotein 35–55 induced EAE animal model of MS. MR images were acquired 14, 25, and 50 days postimmunization. Seed-based analysis was used to investigate the whole-brain FC with some predefined areas, such as the thalamic regions, cerebellum, motor and somatosensory cortex. When compared with the control group, the EAE group exhibited a slightly altered FC and a decreasing trend in the total number of activated voxels along the disease progression. The most interesting result regards the whole-brain FC with the cerebellum. A hyperconnectivity behavior was found at an early phase and a significant reduced connectivity at a late phase. Moreover, we found a negative correlation between the total

Abbreviations: ABA, Allen mouse Brain Atlas; ACC, anterior cingulate cortex; AD, axial diffusivity; BOLD, blood-oxygen level-dependent; CBM, cerebellum; Cpu, caudate putamen; CSF, cerebrospinal fluid; DMN, default mode network; dpi, days postimmunization; EAE, experimental autoimmune encephalomyelitis; En, entorhinal area; FA, fractional anisotropy; FC, functional connectivity; GM, gray matter; HP, hippocampus; IC, inferior colliculus; ICA, independent component analysis; ICs, independent components; LDTh, lateral dorsal thalamus; M1, primary motor cortex; M2, secondary motor cortex; MD, mean diffusivity; MDTh, medial dorsal thalamus; MOG_{35–55}, myelin oligodendrocyte glycoprotein 35–55; MS, multiple sclerosis; OB, olfactory bulb; RD, radial diffusivity; RSC, retrosplenial cortex; rsfMRI, resting-state functional MRI; RSN, resting-state network; S1, primary somatosensory cortex; S1_{BF}, primary somatosensory barrel cortex; S1_{LL}, primary somatosensory lower limb; S1_{UL}, primary somatosensory upper limb; SBA, seed-based analysis; SMA, supplementary somatosensory area; SS, somatosensory cortex; VIS, visual cortex; WM, white matter.

number of activated voxels during the late phase and the cumulative disease index. The results obtained provide a clinically relevant experimental platform that may be pivotal for the elucidation of the key mechanisms of accumulation of irreversible disability, as well as the development of innovative therapies for MS. Moreover, the negative correlation between the disease severity and the size of the activated area suggests a possible research pathway to follow for the resolution of the clinico-radiological paradox.

KEYWORDS

experimental autoimmune encephalomyelitis, functional connectivity, multiple sclerosis, resting-state fMRI

1 | INTRODUCTION

Multiple sclerosis (MS) is an autoimmune neurodegenerative disease targeting white matter (WM) in the central nervous system (CNS). In MS, the immune cells attack the protective sheath of nerve fibers in the CNS, leading to demyelination and axonal damage.¹ As such, remyelination, resolution of inflammation, and functional neuronal reorganization are key factors that may contribute to functional recovery.²

Magnetic resonance imaging (MRI) is essential in diagnosing MS, highlighting demyelinating lesions, CNS inflammation, edema, and axonal damage.³

However, the discrepancy between the severity of clinical symptoms experienced by MS patients and the extent of radiological lesions observed in imaging studies has been reported, laying the foundation for the so-called clinico-radiological paradox.⁴ Some patients may exhibit only mild or moderate symptoms despite having many lesions visible on MRI, while others may have severe symptoms despite few or no visible lesions on MRI. Several factors may contribute to the clinico-radiological paradox in MS. One possible explanation is that not all lesions seen on MRI are functionally relevant or active. Some lesions may be old and inactive, while others may be in areas of the brain that are not crucial for cognitive or motor function. Additionally, some patients may exhibit compensatory mechanisms or functional reorganization that help to mitigate the effects of lesions in critical areas.⁴ Such discrepancy has pushed toward functional MRI (fMRI) studies that allow investigating the functional changes in brain activity and elucidating possible brain plasticity.^{5,6} Since the early 2000s, fMRI studies have demonstrated a reorganization of the cortical areas recruitment during motor, sensory, and cognitive tasks in MS patients.^{5,6} However, factors such as subjective ability in executing tasks, age, gender, different stage of CNS inflammation, and the potential effect of treatments can lead to deceptive interpretation of the task-based fMRI studies in humans.

The analysis of brain functional connectivity (FC) at rest is a possible approach to overcome some of these limitations. Resting-state fMRI (rsfMRI) is a relevant imaging tool that allows to evaluate regional functional interactions within the brain among different brain regions that are spatially distinct. These regions of well-organized brain activity are known as resting-state networks (RSNs).^{7,8} Relevant FC alterations have been reported in MS.^{9,10} Specifically, increased FC at an early stage of the disease has been found in MS patients and interpreted as adaptive brain reorganization, although such an adaptive phenomenon may be present in the early stage of the disease and lost during advanced stages.^{11,12} The rsfMRI approach can be a useful tool with which to classify the disease state in MS patients, with the ultimate aim of identifying new biomarkers to establish prognosis and monitor treatment efficacy.^{13,14}

Experimental models of MS play a crucial role in pharmacological research, from the identification of a therapeutic target to the *in vivo* validation of efficacy. Experimental autoimmune encephalomyelitis (EAE) is the most common animal model of MS, and can be induced in different animal species, including rodents. Myelin oligodendrocyte glycoprotein 35-55 (MOG₃₅₋₅₅) is a potent encephalitogenic peptide in C57Bl/6 (H-2b) mice, and immunization with this peptide leads to chronic progressive disease.^{15,16} Our group has previously demonstrated that functional reorganization of the cerebral cortex in response to somatosensory stimulation occurs in an experimental model of MS in rats.¹⁷ Despite the recognized relevance of fMRI studies in humans,¹⁴ this approach has not been deeply investigated in the EAE model. In the current rsfMRI study we report a longitudinal investigation of FC alterations in the MOG₃₅₋₅₅-induced EAE model of MS. The greatest advantage of rsfMRI is its translational potential; in fact, no stimulus is applied to animals, providing suitable conditions for the analysis of FC using methods analogous to those used in humans. To the best of our knowledge, this is the first rsfMRI investigation of the EAE animal model of MS.

This study aims to validate rsfMRI as a biomarker of the disease progression in the EAE animal model of MS. The results obtained can provide a clinically relevant experimental platform that may be pivotal for the elucidation of key mechanisms of accumulation of irreversible disability and the development/testing of innovative therapies for MS.

2 | MATERIALS AND METHODS

2.1 | Animals and EAE induction

Chronic EAE was induced as previously reported.¹⁸ Briefly, a total of 50 8–10-week-old C57Bl/6 female mice were purchased from Envigo RMS Srl (San Pietro al Natisone, Italy). A group of 27 mice (the EAE group) were immunized by subcutaneous administration with 150 µg of MOG_{35–55} peptide in complete Freund's adjuvant (Becton Dickinson) containing 0.8 mg/mL heat-killed *Mycobacterium tuberculosis* (Becton Dickinson). The mice were also injected intravenously with pertussis toxin (1040 ng; List Biological Laboratories) on the day of immunization and after 48 h. A control (CTR) group of 19 mice received complete Freund's adjuvant and pertussis toxin, but no MOG_{35–55} peptide. Four mice were used in preliminary MRI experiments to set up the acquisition protocol. The mice were housed in pathogen-free, climate-controlled facilities and were provided with food and water according to current European Community laws. All mouse experiments were carried out in accordance with experimental guidelines approved by the University of Verona committee on animal research (Centro Interdipartimentale di Servizio alla Ricerca Sperimentale) and by the Italian Ministry of Health. Protocol numbers 33588, 30969, and 96/2023-PR were used for the in vivo studies in this manuscript.

2.1.1 | EAE clinical score

For clinical signs of the disease, the EAE mice were examined up to 50 days postimmunization (dpi), and the neurological deficits were graded according to a standard 0–5 scale: 0 = healthy; 1 = limp tail (onset of the disease); 2 = ataxia and/or paresis of hind limbs; 3 = paraplegia; 4 = paraplegia with forelimb weakness or paralysis; and 5 = moribund or dead animal.¹⁸ Moreover, to quantify the overall disease severity at the end of the experiment, the cumulative disease index (CDI) was determined by calculating the area under the clinical score curve over time for each animal.¹⁷

2.2 | Preparation for MRI and rsfMRI

For rsfMRI, mice were anesthetized according to a previously published work.¹⁹ Initially, to ensure proper positioning of the mice in the scanner, they were anesthetized with 2% isoflurane (Isoflurane-Vet, Merial, Italy) in a mixture of O₂/N₂ 30/70. Once the mice were correctly positioned, isoflurane anesthesia was slowly discontinued, and a subcutaneous injection of 0.3 mg/kg of medetomidine (Domitor, Pfizer Animal Health, Germany) was administered. Five minutes before the rsfMRI acquisition, the isoflurane level was reduced to 0.4% and maintained at this level during the acquisition of rsfMRI data. For all mice, rsfMRI scans were acquired approximately 25 min after anesthesia induction. For the remaining part of the imaging procedure, isoflurane was newly increased (0.5%–1%). After the imaging procedures, the medetomidine effect was counteracted with the injection of 0.1 mg/kg atipamezole (Antisedan, Pfizer Animal Health, Germany). The anesthesia procedure was maintained consistently across all acquisitions, in accordance with the experimental procedure.¹⁹ The MRI acquisition protocol, described below, lasted approximately 50 min. The respiratory rate, body temperature, and ECG rate were continuously monitored using a PC-SAM Small Animal Monitor, and the blood pCO₂ level was additionally monitored using a TCM4 Transcutaneous Blood Gas Analyzer (Radiometer). During the imaging session, these parameters remained within a physiological range, guaranteeing the sedation of each animal and the reproducibility of this protocol. Specifically, the mean value of body temperature across all subjects and time points was 36.4 ± 0.01°C, while the mean value of pCO₂ was 66.2 ± 1.1 mmHg, and the mean respiratory rate was 95.2 ± 1.5 breaths/min (values reported as mean ± SEM). Mice outside these ranges were discarded. A total of six mice were discarded.

2.3 | MRI acquisition

Images were acquired using a Bruker Biospec tomograph (Bruker, Ettlingen, Germany) operating at 7 T and a cross-coil configuration. A 7.0-cm internal diameter, bird cage volume coil was used for transmission and a helmet-shaped surface coil specific for the mouse brain was used as receiver. The scanner was operated using Paravision, version 6.0.1 (Bruker). The MRI acquisitions were performed in the following order: localizer acquisition, rsfMRI, diffusion tensor imaging (DTI), and T₂-weighted anatomical scans.

RsfMRI was performed with a single shot echo planar imaging (EPI) sequence with the following parameters: TR = 1200 ms, TE = 11 ms, MTX = 80 × 80, number of slices = 24, slice thickness = 0.5 mm, FOV = 20 × 20 mm², 300 volumes, and total acquisition time = 6 min. A single EPI sequence with reversed phase-encode blips was also acquired for the correction of susceptibility-induced distortions.

DT images were acquired with an EPI sequence with the following parameters: TR = 1200 ms, TE = 24.5 ms, MTX = 192×192 , number of slices = 24, slice thickness = 0.5 mm, FOV = 20×20 mm², EPI segments = 2, 30 diffusion directions at $b = 1000$ s/mm² and three b₀ images, and total acquisition time = 33 min 36 s. A set of b₀ images with reversed phase-encode blips were also acquired for correction of susceptibility-induced distortions.

T₂-weighted anatomical images were acquired with a rapid acquisition with relaxation enhancement (RARE) sequence with the following parameters: TR = 5960 ms, TE_{eff} = 39 ms, MTX = 256×256 , number of slices = 48, slice thickness = 0.25 mm, FOV = 20×20 mm², RARE factor = 8, NEX = 4, and total acquisition time = 9 min 32 s.

2.4 | MR image processing

All MR images were converted to NIFTI file format, and the voxel size was scaled with a 10x factor to be compliant for subsequent processing.

Structural T₂-weighted images were analyzed with FMRIB Software Library (FSL),²⁰ similar to our previous work.^{21,22} Briefly, total brain tissue, gray matter (GM), WM, cerebellar cortex, striatum, and intraventricular cerebrospinal fluid (CSF) were segmented to obtain their volumes.

DTI data were denoised with MRtrix3²³ and corrected for susceptibility-induced distortions with *topup*²⁴ (part of FSL) using the reversed phase-encode blips images. Eddy current-induced distortions and subject movements were corrected with *eddy*²⁵ (part of FSL). DT images were then fitted with the diffusion tensor model with *dtifit* (part of FSL) to obtain fractional anisotropy (FA), mean diffusivity (MD), axial diffusivity (AD), and radial diffusivity (RD).

RsfMRI data were first corrected for susceptibility-induced distortions with *topup* using the reversed phase-encode blips images. The preprocessing was then carried out similarly to our previous work.^{26,27} Briefly, the preprocessing was run with the MELODIC tool of FSL and consisted of motion correction, slice timing correction, and spatial smoothing with a full width at half maximum of 5.0 mm. Functional data were then analyzed with independent component analysis (ICA) and the resulting components were manually labeled as true signal or noise in 14 subjects (seven CTR and seven EAE) randomly chosen in our dataset-artifact signals,^{28,29} to identify the RSNs in the functional data and to regress out the noise from the full dataset (84 MRI acquisitions). FIX was run with the *-m* option to additionally clean up the motion confounds.

2.5 | Data analysis

The Allen mouse Brain Atlas (ABA; <https://mouse.brain-map.org/>) was nonlinearly registered to T₂-weighted images then mapped onto rsfMRI and DT images with a second linear registration step to obtain a parcellation of the brains in each subject space. The parcellation consisted of 49 regions of both WM and GM.

Whole-brain, cerebellar cortex, striatum, and total intraventricular CSF volumes were calculated for each subject at each time point according to T₂-weighted images segmentation and ABA parcellation.

The mean values of the FA, MD, AD, and RD parameters were calculated for each subject at each time point in the WM and GM regions according to ABA parcellation.

2.5.1 | Analysis of rsfMRI data

Independent component analysis

To estimate FC, a group ICA was performed in the preprocessed and normalized dataset using GIFT v. 3.0b (Group ICA of fMRI toolbox: <https://trendscenter.org/software/>), working in MATLAB (version 2022a; MathWorks). The analysis was performed multiple times with varying numbers of independent components (ICs) (i.e., 15, 20, 25, 30, 35, and 40). Ultimately, the number of ICs was set to 40 because it preserved the spatial information while maintaining the integrity of fMRI signals in identifiable neuroanatomical systems.³⁰ Group ICA was carried out using the Infomax algorithm, with no autofill of data reduction values, variance normalization as data preprocessing type, a brain mask to remove nonbrain signal, and GICA as the back reconstruction method. All the other parameters were set as default. The spatial ICs maps were scaled to Z-scores with a threshold of $|Z|$ more than 1.7 (corresponding to uncorrected $p < 0.05$, two-tail test).³¹ ICs were overlaid onto the mouse ABA to aid structural identification and were named according to the regions they overlapped with. Finally, the ICs maps were visually inspected, and a component classification was performed based on a defined set of rules.³² A component was considered acceptable if: (i) it was characterized with bilateral organization or, at least, unilateral with a corresponding separate contralateral component; (ii) a low number of large clusters localized in the GM and continued across slices; and (iii) very low or absent overlap with WM, CSF, blood vessels, and brain boundaries. Consequently, components characterized with a large number of small noncontiguous clusters, high overlapping with one or more of WM, CSF, blood vessels, and brain boundaries, were classified as noise components and discarded.^{32,33} The set of spatial maps from the group-average analysis was used to generate

subject-specific versions of the spatial maps and associated time series, using dual regression (part of FSL).³⁴ First, for each subject, the group-average set of spatial maps was regressed (as spatial regressor in a multiple regression) into the subject's 4D space-time dataset. This resulted in a set of subject-specific time series, one per group-level spatial map. Next, those time series were regressed (as temporal regressors in a multiple regression) into the same 4D dataset, resulting in a set of subject-specific spatial maps, one per group-level spatial map. Finally, FC group differences were tested using FSL's randomize permutation-testing tool with 10,000 permutations.^{34,35}

Seed-based analysis

The ICA-based cleaning functional data were used as the input for the seed-based analysis (SBA).³⁶ Data processing was conducted using FSL/FEAT.^{37–39} Seed regions were selected based on anatomical structures belonging to networks of interest observed in the ICA maps. Five bilateral seeds of 27 voxels placed with a spherical pattern were manually traced on coronal sections in the primary motor cortex (M1), primary somatosensory barrel field cortex (S1_{BF}), cerebellum (CBM), medial dorsal thalamus (MDTh), and lateral dorsal thalamus (LDTh), using the mouse ABA as template (see Figure S1). To generate an individual whole-brain correlation map,³⁸ the average time series were extracted from each seed and correlated with the time series of all voxels in the brain. Group-level analyses^{37,39} were performed for each seed region using a mixed effects FLAME 1 model and a two-groups unpaired *t*-test. Z statistic maps of clusters, for both individual and group analyses, were defined by a Z threshold of more than 3.1 and a corrected cluster P threshold = 0.05 using Gaussian Random Field theory.⁴⁰

2.6 | Statistical analysis

To detect differences between the CTR and EAE groups in DTI and volumetric data, the statistical analysis was carried out in MATLAB (version 2022a; MathWorks) with a mixed-effects model approach to cope with repeated measurements and random missing data because of experimental limitations. Statistical analysis was corrected for multiple comparisons with the Bonferroni method.

Statistical analysis of rsfMRI data was performed with OriginPro, Version 2022 (OriginLab Corporation, Northampton, MA, USA).

The mean z-stat value from the subject whole-brain correlation map was used to define the FC value. The Kruskal-Wallis test was employed to assess statistical differences in longitudinal FC values within both the CTR and EAE groups. Bonferroni's adjustment was applied to compensate for multiple comparisons. The Mann-Whitney-Wilcoxon test was used for group comparisons, that is, to test differences between the CTR and EAE groups at each time point, with the null hypothesis being median1 = median2.

The correlation between CDI and all MRI-derived parameters (FA, MD, RD, AD, total number of activated voxels, and z-stat value) was assessed using Pearson's correlation coefficient (*r*). Moreover, the same procedure was applied to investigate the correlation between the rsfMRI and DTI parameters.

For all the statistical analyses conducted, a *p* value below 0.05 was regarded as statistically significant. Values reported are expressed as mean ± SEM.

3 | RESULTS

3.1 | EAE development

EAE disease development is shown in Figure 1A. In most mice, the first episode of tail weakness occurred between 9 and 16 dpi. The peak of EAE clinical severity was considered as the time point at which mice exhibited paraplegia and it was reached at 22–25 dpi. An incomplete remission of clinical disabilities persisted up to 50 dpi during the chronic phase of disease. Thus, the EAE deficits persisted during the disease, showing however a minor severity during the late chronic phase. Overall, the EAE score was in line with our previously reported data.¹⁸

3.2 | Morphological imaging

Whole-brain, CBM, striatum, and intraventricular CSF volumes analysis, based on T₂-weighted images (representative EAE mouse brain in Figure 1B), did not reveal statistically significant differences between groups at any time point. Additionally, the time evolution of the analyzed volumes did not differ between the CTR and EAE mice. The average volumes of the whole-brain, CBM, striatum, and intraventricular CSF structures of both CTR and EAE mice are reported in Figure 1C,D,E,F, respectively. Moreover, comparative brain volumetry of GM and WM did not show any statistically significant difference between groups at any time point.

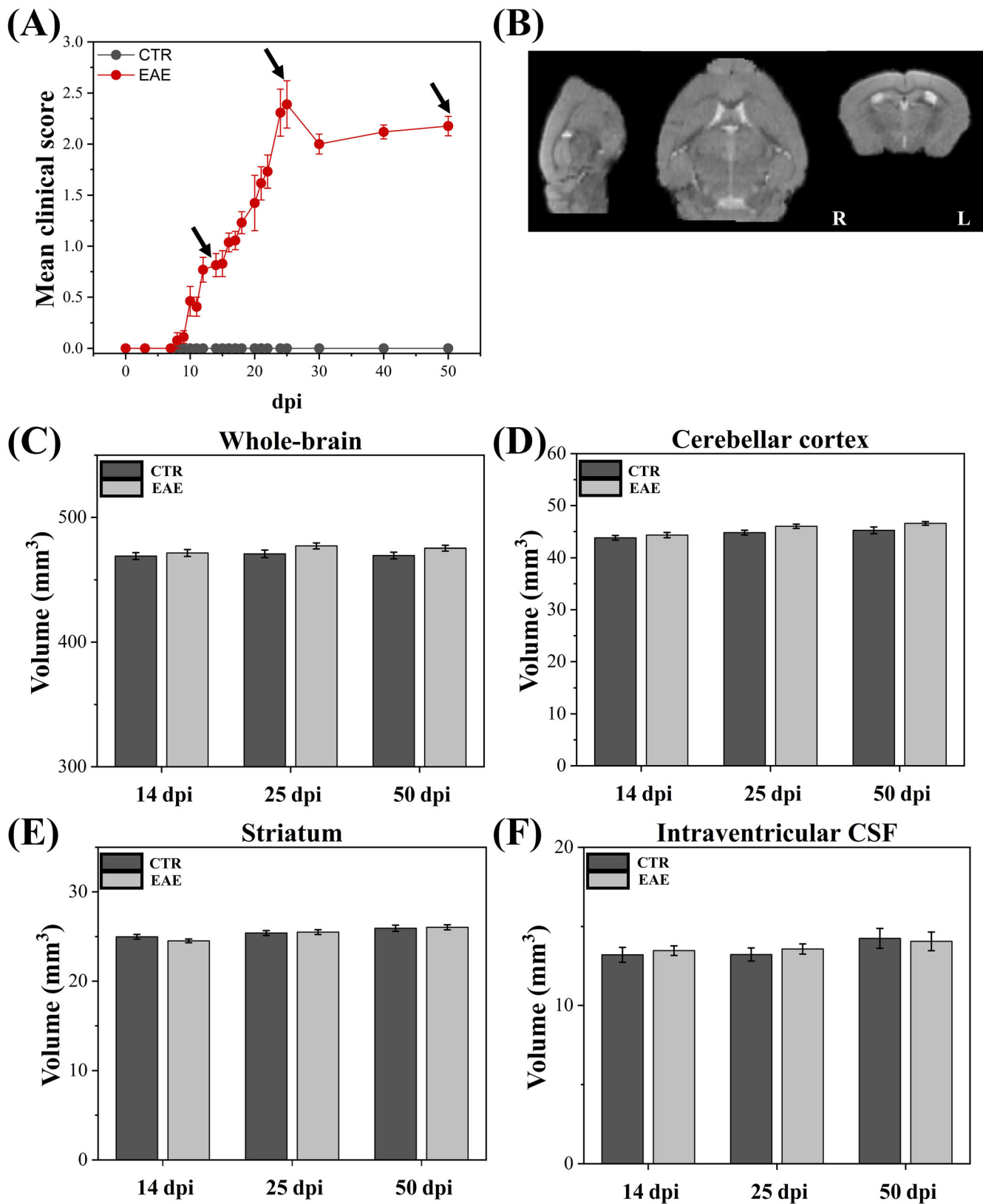


FIGURE 1 Clinical score recorded along with EAE course and cerebral volumes. (A) Time course of clinical score in control (CTR) and EAE groups up to 50 days postimmunization (dpi). The black arrows indicate the day upon which all the mice underwent MR acquisition. (B) Representative T₂-weighted MR images of an EAE mouse. (C) Quantification of whole-brain, (D) Cerebellar cortex, (E) Striatum, and (F) Intraventricular CSF volumes of CTR and EAE mice determined at different time points. All data are represented as mean \pm SEM. No statistically significant difference was identified between the groups. CSF, cerebrospinal fluid; EAE, experimental autoimmune encephalomyelitis.

3.3 | Diffusion tensor imaging

The analysis of DTI-derived metrics revealed that MD and RD in WM regions, namely, brainstem (medulla and pons), corpus callosum, and corticospinal tract, showed a time trend that was significantly different ($p < 0.05$) in CTR versus EAE mice. Specifically, the MD and RD values of WM regions showed a positive trend over time in EAE mice ($1.50 \times 10^{-6} \text{ mm}^2/\text{s} \cdot \text{day}^{-1}$, Figure 2B on the right, and $1.45 \times 10^{-6} \text{ mm}^2/\text{s} \cdot \text{day}^{-1}$, Figure 2C on the right, respectively), while in CTR mice the trend was not significantly different from zero (Figure 2B and Figure 2C, both on the

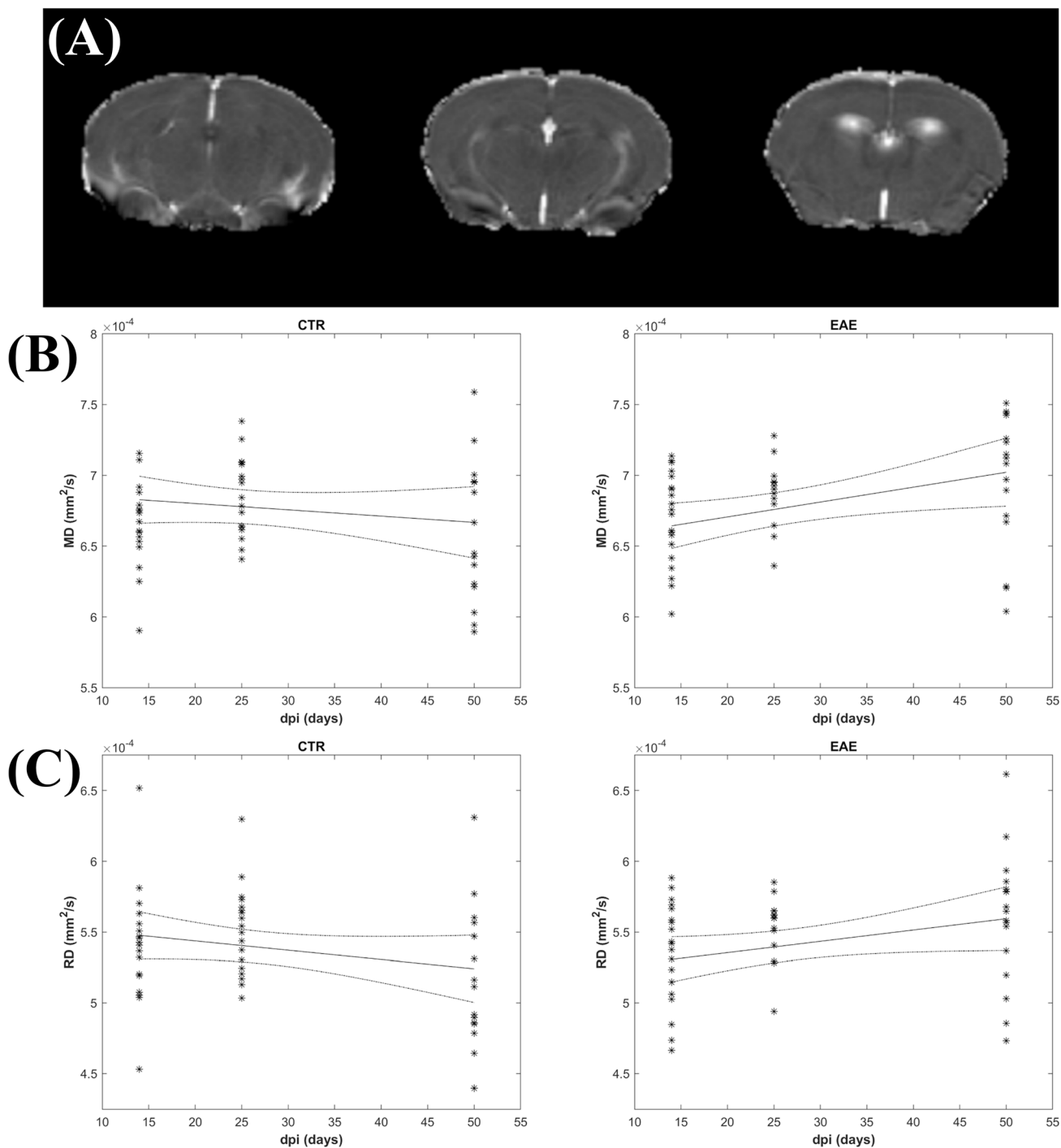


FIGURE 2 DTI results. (A) Representative MD maps of three axial slices. (B) Time evolution of MD in WM regions of the CTR group on the left and the EAE group on the right. (C) Time evolution of RD in WM regions of the CTR group on the left and the EAE group on the right. CTR, control; dpi, days postimmunization; DTI, diffusion tensor imaging; EAE, experimental autoimmune encephalomyelitis; MD, mean diffusivity; RD, radial diffusivity; WM, white matter.

left). Groupwise differences became significant ($p < 0.05$) at the third time point, that is, 50 dpi, when MD and RD in EAE mice was higher than in CTR mice (7.02×10^{-4} vs. 6.59×10^{-4} mm²/s and 5.60×10^{-4} vs. 5.18×10^{-4} mm²/s, respectively). No group differences were found in either FA or in AD. As far as GM is concerned, no group differences were found in all parameters. No correlation was observed between DTI parameters and CDI.

3.4 | Resting-state functional MRI

3.4.1 | Independent components analysis

Group ICA was performed using 40 components. After visual inspection, following the rules for ICA classification previously reported in the ICA paragraph of the Materials and Methods section, 10 components were classified as being of non-blood oxygen level-dependent (BOLD) artifactual origin and the remaining 30 components as signal-component. When compared with known neuroanatomical regions, most of the signal-components showed a strongly symmetric interhemispheric connectivity, comparable with the functional networks reported in previous rsfMRI studies of mouse brain.^{31–33} Bilateral components that overlapped onto cortical and subcortical areas were found in several regions, including the M1, somatosensory cortex (SS), auditory cortex (Au), retrosplenial cortex (RSC), visual cortex (VIS), olfactory bulb (OB), CBM, inferior colliculus (IC), amygdala, and medial septal nuclei (Figure 3). It should be noted that RSC and VIS are involved in the default mode network (DMN), a network identified in the rest condition.⁴¹ The components that properly matched the hippocampus (HP), caudate putamen (Cpu), and entorhinal area (En) were split up in two or more components (see Figure S2). These networks were consistently identified in both the CTR and EAE groups. No statistically significant difference was detected between groups at each time point.

3.4.2 | Seed-based analysis

Because we had prior knowledge regarding which regions may be affected, based on human and murine studies, we applied SBA. As specified in the Materials and Methods section, seeds were placed in regions known to be involved in human MS or in the EAE model,¹⁷ like the motor cortex, SS, cerebellum, and thalamus. The group-level maps showed that both the CTR and EAE groups exhibited interhemispheric and intrahemispheric connectivity. The FC was estimated as the mean z-stat value calculated from individual whole-brain correlation maps. Figure 4 reports the results obtained by placing the seeds in the CBM. In Figure 4A, the 3D reconstruction of activated voxels is reported at different time points for the CTR and EAE groups. The brain areas correlated with the seeds for the CTR group at all time points were identified in the anterior cingulate cortex (ACC), M1, the secondary motor cortex (M2), SS, posterior parietal association area, VIS, dorsal striatum, and RSC. Interestingly, all these regions were also highlighted in the EAE group at 14 and 25 dpi, with a diffuse involvement of the whole cortical area and the CBM, mainly at the onset of the disease. At 50 dpi, the EAE group revealed that correlation with the seeds was weakly maintained only with the M1 and VIS. Visually, the maps in Figure 4A show that the number of activated voxels tends to remain constant over time in the CTR group, while a decreasing trend can be observed in the EAE group. Quantitative values obtained from such group-level maps are reported in Figure 4B. In Figure 4C, the quantitative data obtained from the activation maps are reported by calculating the mean z-stat value. The z-stat value was significantly different in the EAE group between 14 and 50 dpi. Although a decreasing trend could be visually observed in the CTR group, no statistically significant difference was found in this group over time. Moreover, it is interesting to note that at 14 dpi the number of activated voxels is much higher in the EAE group (Figure 4B), while the mean z-stat value is lower (Figure 4C). Finally, there was a statistically significant correlation between the number of activated voxels and CDI ($r = -0.70$, $p = 0.007$) at 50 dpi (Figure 4D).

Figure 5 summarizes the results obtained by placing the seeds in other brain regions: the M1 (A), S1_{BF} (B), and LDTh (C). Each panel shows the 3D reconstruction of activated voxels and the relative mean z-stat value. Panel (A) of Figure 5 reports the results obtained by placing the seeds in the M1. In the CTR group, the BOLD fMRI signal of the motor cortex is highly correlated with S1_{BF}, dorsal striatum, Au, RSC, VIS, and CBM. These correlations were maintained at 25 and 50 dpi. The same areas were also identified in the EAE group at 14 dpi, with reduced involvement of VIS and SS compared with the CTR group. Qualitatively, it is noticeable that there is a decreasing trend in the number of activated voxels in the EAE group along the disease progression, with reduced involvement of CBM and VIS, especially at 50 dpi. Quantitative data show that the FC, measured from z-stat values, was statistically significantly lower for the EAE than for the CTR group at 14 dpi ($p < 0.05$). No other statistically significant differences were detected between the groups.

Panel (B) of Figure 5 is similar to panel (A), but refers to seeds in the S1_{BF}. In the CTR group, we observed a strong correlation with the other area of SS, for example, the upper limb (S1_{UL}) and lower limb (S1_{LL}), supplementary somatosensory area (SMA), M2, RSC, VIS, and ventral Au. These regions were also identified in the EAE group at 14 dpi. Qualitatively, it was appreciable a decreasing trend in the number of activated voxels in the EAE group over the course of the disease progression. No statistically significant differences in mean z-stat values were found between the CTR and EAE groups at any time point.

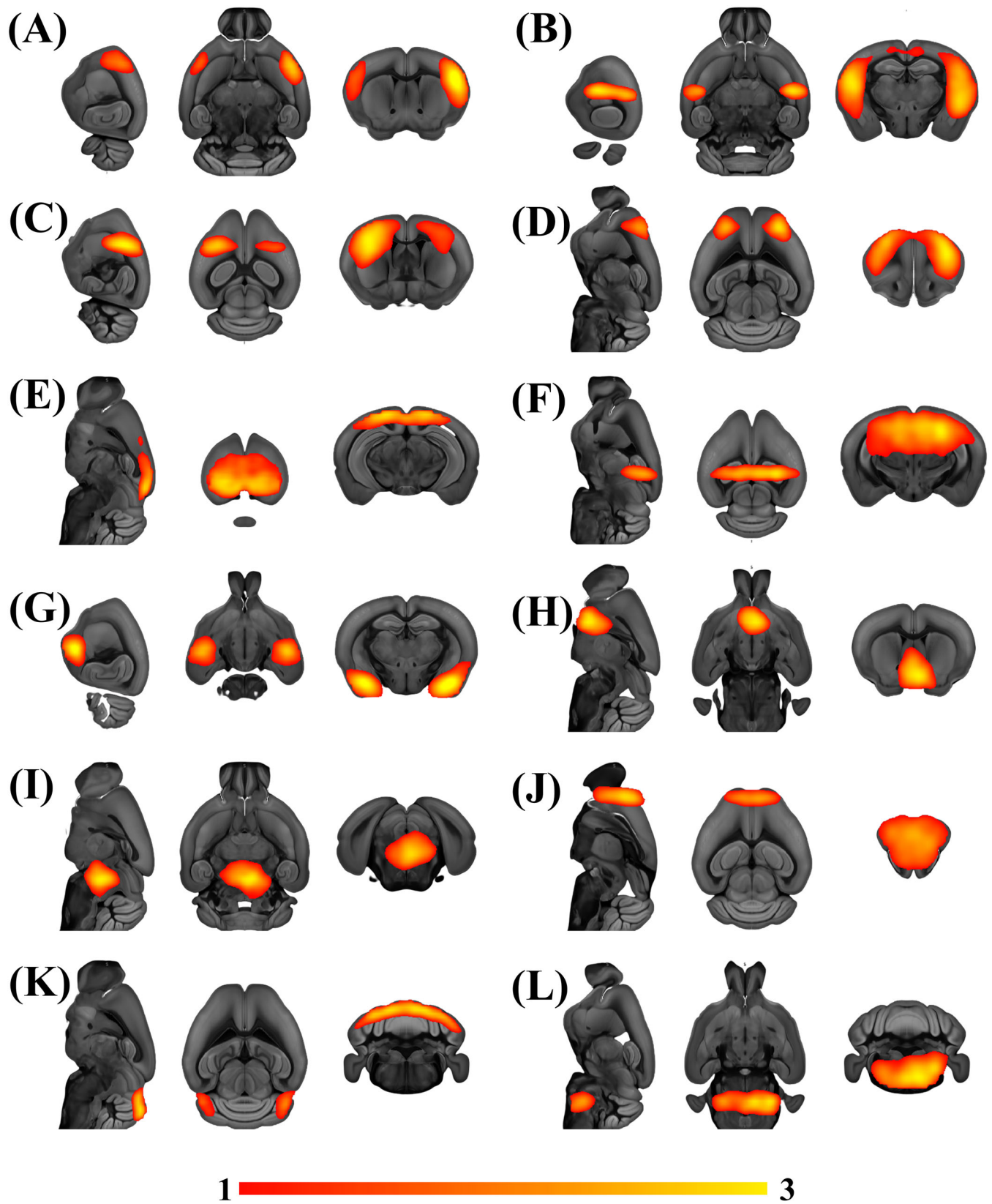


FIGURE 3 Legend on next page.

FIGURE 3 Spatial maps of bilateral functional connectivity resulting from 40 components group ICA (GIFT) of rsfMRI. The spatial color-coded z-maps of the components are overlaid on the Allen mouse Brain Atlas (ABA). According to the mouse ABA parcellation, the resting-state networks were found in the cortex, cerebellum, basal ganglia, and limbic system. (A) Primary somatosensory cortex (S1), mouth; (B) Auditory cortex (Au); (C) Primary somatosensory cortex, upper limb (S1_{UP}); (D) Primary motor cortex (M1); (E) Retrosplenial cortex (RSC) and visual cortex (VIS); (F) Ventral hippocampus (HP); (G) Amygdala; (H) Medial septal nuclei; (I) Midbrain, motor related; (J) Olfactory bulb (OB); (K) Cerebellar cortex, inferior colliculus (IC); (L) Medulla, motor related. All the components are shown in radiological convention. ICA, independent component analysis; rsfMRI, resting-state functional MRI.

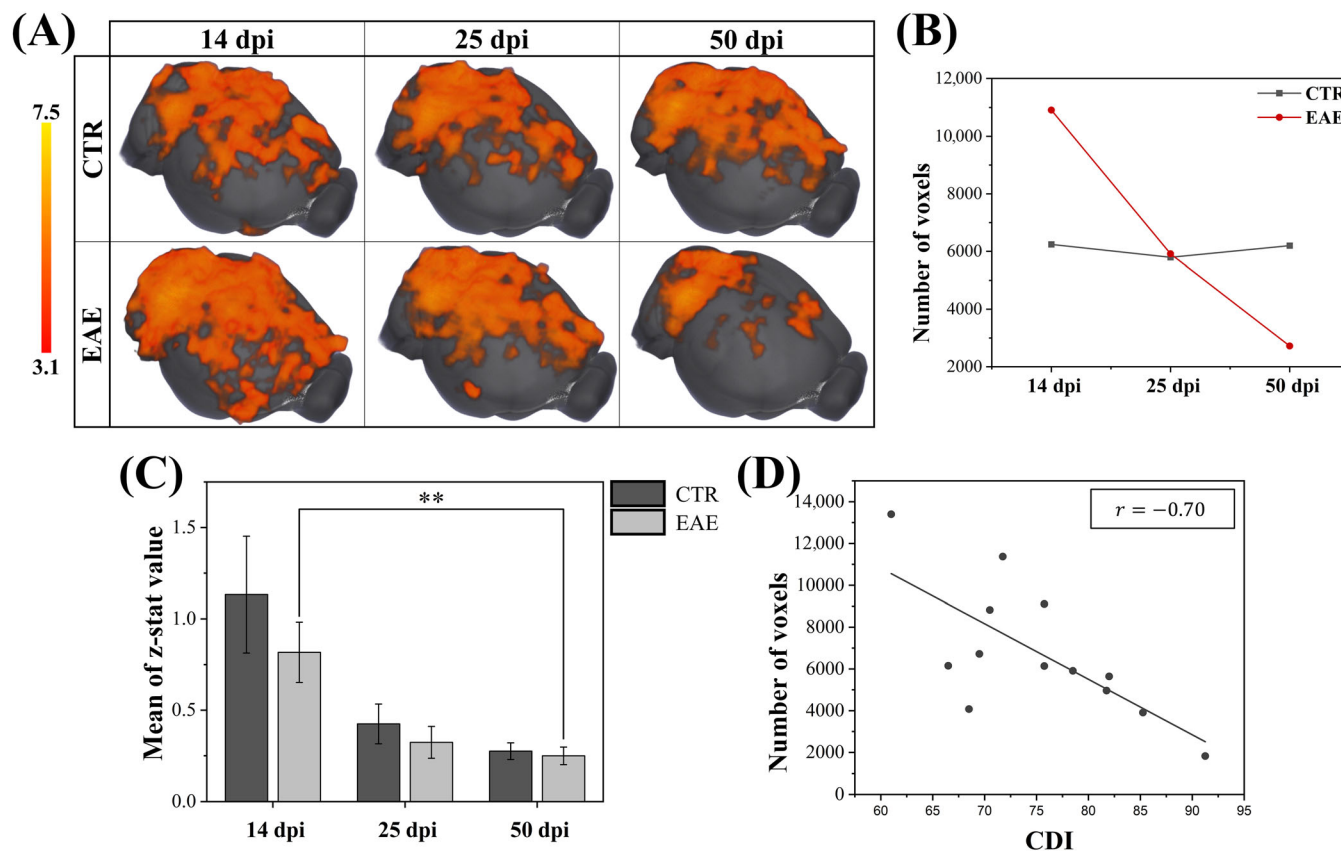


FIGURE 4 Seed-based analysis performed with seeds in the cerebellum. (A) Group-level maps of functional connectivity obtained from the analysis at 14, 25, and 50 days postimmunization (dpi) in both control (CTR) and EAE groups. The spatial color-coded z-maps are overlaid on the Allen mouse Brain Atlas. (B) Number of activated voxels related to panel (A). (C) Average functional connectivity value obtained from z-stats maps of each subject at 14, 25, and 50 dpi. ** $p < 0.01$. (D) Correlation between the number of activated voxels at 50 dpi and the corresponding cumulative disease index (CDI) calculated for each subject at 50 dpi. Total number of acquisitions: CTR = 41, EAE = 43. EAE, experimental autoimmune encephalomyelitis.

Panel (C) of Figure 5 shows the seed-based connectivity between the LDTh and the whole brain. At 14 dpi, in the EAE group, the brain areas correlated with the LDTh were hippocampal commissure, hypothalamus, HP, orbital area, ACC, and S1_{BF}. At 25 and 50 dpi, the number of correlated areas decreased, and the LDTh region was only correlated with the hippocampal commissure and HP, as observed in the CTR group at all time points. Along the disease progression, the FC significantly decreased between 14 and 50 dpi. These findings resemble results reported in human MS, as we will discuss in more detail in the Discussion section. Similar findings were observed in the case of seeds placed in the MDTh (see Figure S3).

In the three cases presented in Figure 5, no statistically significant differences were found in the z-stat values for the CTR group over time. Moreover, at 50 dpi, no correlation was observed between the rsfMRI-derived parameters and CDI in the EAE group.

Finally, no correlation was observed between the number of activated voxels and DTI parameters, at all time points.

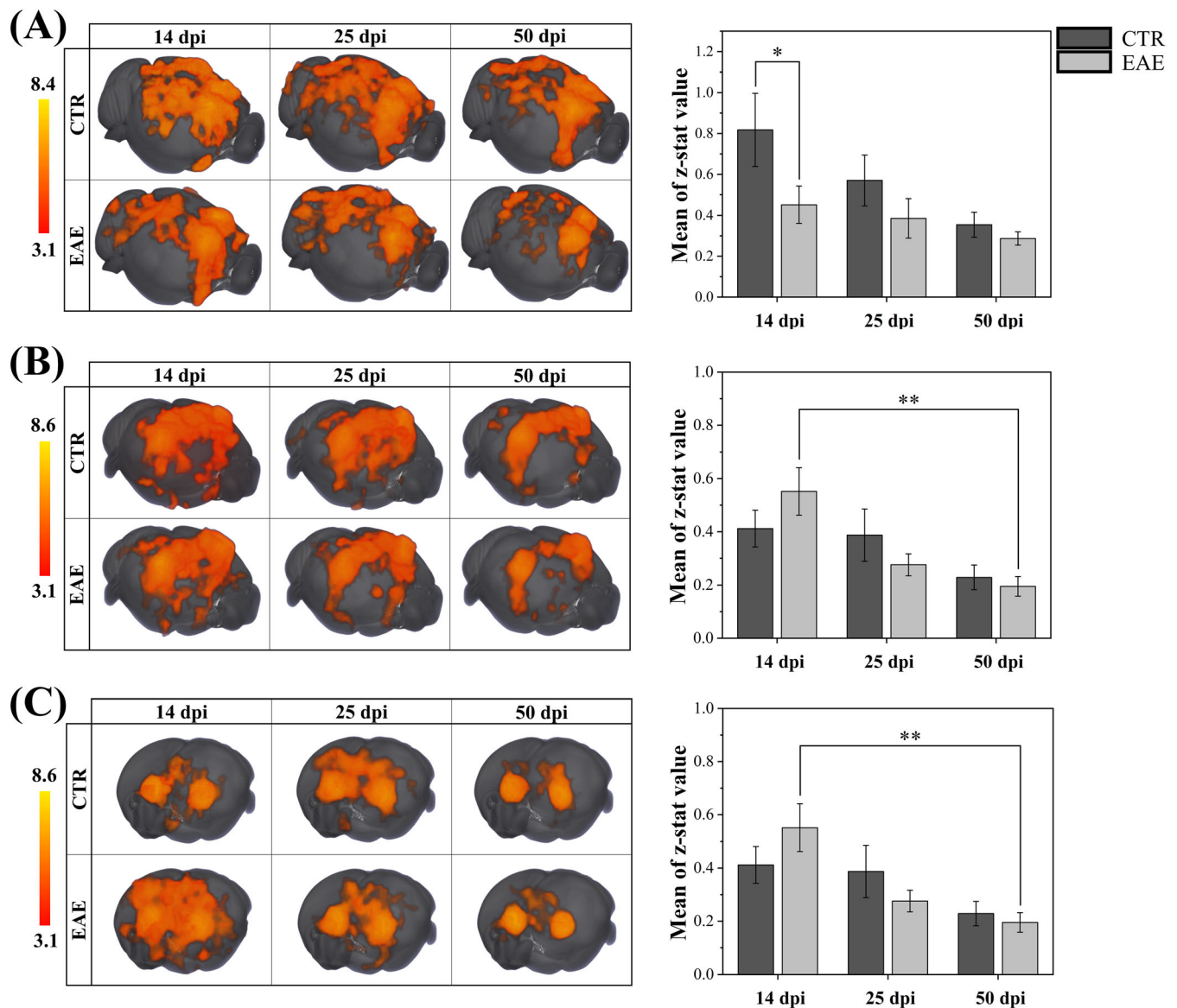


FIGURE 5 Seed-based analysis performed with seeds in the motor cortex, somatosensory cortex, and lateral dorsal thalamus. (A) On the left: group-level maps of functional connectivity obtained by placing seeds in the motor cortex from the analysis at 14, 25, and 50 days postimmunization (dpi) in both control (CTR) and EAE groups. The spatial color-coded z-maps are overlaid on the Allen mouse Brain Atlas. On the right: average functional connectivity value obtained from z-stats maps of each subject at 14, 25, and 50 dpi. $*p < 0.05$. (B) On the left: group-level maps of functional connectivity obtained by placing seeds in the somatosensory cortex. On the right: average functional connectivity value obtained from z-stats maps of each subject. (C) On the left: group-level maps of functional connectivity obtained by placing seeds in the lateral thalamus. On the right: average functional connectivity value obtained from z-stats maps of each subject. $**p < 0.01$. Total number of acquisitions: CTR = 41, EAE = 43. EAE, experimental autoimmune encephalomyelitis.

4 | DISCUSSION

EAE is a widely used experimental model of autoimmune inflammatory disease of the CNS, and, despite having some limitations, it mimics several aspects of human MS. In particular, the clinical signs of the EAE model, such as motor weakness, ataxia, and spasticity, resemble those observed in MS patients. Additionally, the pathological features of EAE, including inflammation, demyelination, and axonal damage, mirror those seen in human MS.¹⁶ Moreover, because of the incomplete resolution of inflammation and demyelination after the disease peak, the MOG_{35–55}-induced EAE model used in this study represents a suitable tool for the study of chronic inflammatory demyelination, resembling the one experienced by MS patients. Indeed, past investigation conducted exploiting this experimental model has contributed to a deeper understanding of the MS-associated pathological processes and also to the development of drugs currently used to treat patients.^{42–45} The EAE mouse model is mainly used to study structural damage and could provide a way to investigate the mechanisms that lead to inflammatory processes, demyelination, and

axonal lesions in human MS.¹⁶ This allows researchers to study the mechanisms contributing to the development of MS symptoms and gain new insights into its pathological processes, favoring the identification of new treatment strategies. The EAE model has been shown to reflect the polygenic and multifactorial nature of MS in humans,⁴⁶ and a genome-wide study on an EAE model using a similar induction protocol with MOG₃₅₋₅₅ peptide in adjuvant supplemented with *Mycobacterium tuberculosis* identified linkages on 18 chromosomes harboring loci controlling EAE, thus highlighting the genetic underpinnings of this model.⁴⁷

MRI is a powerful imaging tool largely used in human MS to detect lesions in the CNS.³ Despite the recognized relevance of fMRI studies in humans,¹⁴ this approach has not been deeply investigated in the EAE model.

To the best of our knowledge, this study is the first to explore rsfMRI to define innovative biomarkers of the EAE disease progression. In this longitudinal MRI study, performed at three time points (14, 25, and 50 dpi), we focused on the effect the EAE model had on the brain and its functional organization.

Resting-state data were analyzed with two approaches, namely, ICA, to investigate RSNs, and SBA, to investigate whole-brain FC with some predefined brain areas (the M1, S1_{BF}, CBM, and thalamic regions). While the first approach did not reveal group differences in RSNs, the SBA revealed that the FC of the EAE group exhibited slight alterations compared with the CTR group. Specifically, whatever the area under investigation is, a decreasing trend in the total number of activated voxels was observed in the EAE group as the disease progressed.

The main outcome focused on the whole-brain FC with the cerebellar area. The SBA in the CTR group revealed that the CBM was functionally connected with the motor area, ACC, RSC, dorsal striatum, SS, and VIS at rest. Interestingly, at the onset of the disease, EAE mice showed increased and more distributed brain activation of the whole cortical area and the CBM, but with lower strength compared with the CTR group. This suggests an initial compensatory mechanism where the brain recruits wider brain regions to limit the functional effects of the pathology. However, during the late chronic phase, the FC between the CBM and the whole brain significantly decreased, possibly indicating that the cumulative damage impairs the CBM's ability to maintain such FC. Indeed, a negative correlation was found between the number of activated voxels and CDI calculated for each subject at 50 dpi. Consequently, because a higher CDI value translates to higher disease severity, we found that the higher the disease severity, the lower the total number of connected voxels. These results suggest alterations in the CBM that modify its FC with the whole brain and are correlated with the disease severity. It is well known that the main effect provoked by this EAE mouse model is the demyelination in the WM of the spinal cord, which leads to gradual loss of motor function and the manifestation of clinical disability. Moreover, another important outcome of this EAE model is inflammation of meninges and perivascular inflammatory cuffing in the cerebellum and hindbrain WM.⁴⁸ Recently, widespread reduction of neuron, myelin, and axonal density in the cerebellum with long-term disease was reported in MOG₃₅₋₅₅ EAE-induced mice (66 days after induction).⁴⁹

The whole-brain FC with the seeds placed in the M1, S1, and the thalamic regions showed only marginal alterations between the EAE and the CTR groups. In the thalamus, there was an initial increase in the number of activated voxels compared with the CTR group, and the FC showed a significant decreasing trend as the disease progressed. EAE also induced a decrease in the correlation between the M1 and whole brain during the early phase of the pathology.

It is well known that, in the human brain, the damage caused by MS lesions can lead to a functional rearrangement to adapt to the new condition. An abnormal FC was found in several fMRI and rsfMRI studies conducted on patients affected by MS.¹⁴ These studies reported a mixed pattern of increased and decreased seed-based FC. In MS, the cerebellum is one major site of disease pathology, leading not only to motor disability and balance deficit, but also to cognitive dysfunction.⁵⁰ Several rsfMRI studies, conducted in humans to examine the FC between different cerebellar areas and the entire brain, showed that this connectivity was altered.⁵¹⁻⁵⁴ Our study showed an altered connectivity between the cerebellum and the whole brain, characterized by an initial hyperconnectivity that was waning as the disease progressed. The early hyperconnectivity was also found in some humans studies, and it was interpreted as a need to recruit new regions to compensate for the deficit.^{51,55} It has been reported that functional changes in the human brain may result from structural changes not only in the cerebellum, WM, or GM, but also in the deep GM, especially in the thalamic regions.⁵⁶ In fact, the thalamus plays an important role in cognitive functions, which are impaired in human MS. For this reason, several studies have focused their attention on the investigation of FC alteration for the thalamus^{57,58} and its subregions.^{59,60} Compared with healthy subjects, the findings of these studies indicated abnormality in the FC of the thalamus with the whole brain, resulting in cognitive dysfunctions that affect patients with MS. Therefore, considering the role played by the thalamus within the brain network of humans MS, we decided to inspect the FC between the thalamus and whole brain in the EAE animal model of MS. The EAE group showed both an initial increase in FC and recruitment of brain regions that were not involved in the CTR group, and this behavior resembles what was observed in the human studies cited above.⁵⁷⁻⁶⁰ Comprehensively, our rsfMRI findings suggest that the whole-brain seed-based FC of the EAE group increases at the onset of the disease, followed by a progressive decrease. This early hyperconnectivity behavior is consistent with observations in MS patients, where increased connectivity at disease onset may be related to an early compensatory mechanism that subsequently fails with the progression of brain injury.¹¹

While rsfMRI enables studying the functional architecture of the brain, DTI allows highlighting microstructural damage in the brains of patients affected by MS.⁶¹ DTI was also largely applied in the EAE mouse model, specifically to detect the demyelination and the axonal damage of WM spinal cord and optic nerve.⁶²⁻⁶⁴ Our DTI analysis focused on the brain and revealed that MD and RD values of WM regions, such as the brainstem, corpus callosum, and corticospinal tract, increased as the disease progressed. An increase in the RD parameter was reported in the

studies mentioned above,^{62–64} and was histologically associated with the loss of myelin membrane integrity. MD measures overall water motion, and the increase of this parameter is a common finding in human MS. In particular, an increase of MD was related to the disruption of the myelin sheath and axonal loss, resulting in increased water motion.⁶⁵

Lastly, the volumetric analysis found no statistically significant differences in the whole-brain, cerebellar cortex, striatum, and intraventricular CSF volumes. This finding is different compared with some studies reported in the literature. For example, Smith et al. reported that MRI brain volumetry performed in a similar EAE model revealed a significant decrease in the aforementioned volumes.⁶⁶ However, it must be considered that different protocols for EAE induction may lead to different outcomes. For example, the peak of EAE in the current study comes at around 25 dpi, while in the study conducted by Smith et al. the peak occurs at around 14 dpi. Moreover, Smith et al. observed EAE mice until 126 dpi and the differences tended to be more pronounced at the last time points, while in the current study the mice were only observed up to 50 dpi. Considering all of this, it is possible that our model is progressing more slowly and that we are observing an earlier phase of the disease, as opposed to the observations made by Smith et al.⁶⁶ Of course, this would represent a limitation of our protocol, but one which could be addressed in further studies by extending the observation period. Other studies revealed subtle differences in whole-brain volume reduction along the disease progression in the EAE mouse model.^{67,68} However, those studies focused on high-resolution morphological imaging, adopting high field imager and high SNR cryogenic probes prioritizing spatial resolution. In our study, the main goal was to characterize the EAE mouse model from a microstructural and functional perspective, dedicating most of the imaging time to rsfMRI and DTI, thus reducing the time available for morphological imaging.

In conclusion, rsfMRI could be an innovative biomarker of the EAE mouse model of MS. In this mice group, we identified alterations in FC between the whole brain and the cerebellar and thalamic regions. Specifically, the FC between the cerebellum and whole brain exhibited a more widespread activation during the early stage of the disease, which gradually decreased as the disease progressed. These alterations could be exploited to test the efficacy of innovative treatments aimed at restoring normal FC in the diseased brain. Additionally, we found that the disease severity negatively correlates with the size of the activated area, thus suggesting a possible research pathway to follow for the resolution of the so-called clinico-radiological paradox.

ACKNOWLEDGMENTS

MRI experiments were performed at the Centro Piattaforme Tecnologiche (CPT, University of Verona), with the help of Elena Nicolato, University of Verona, which is gratefully acknowledged. This work was supported by Fondazione Italiana Sclerosi Multipla, Grant 2019/PR-Single/034.

CONFLICT OF INTEREST STATEMENT

None of the authors have any conflicts of interest associated with this study.

ORCID

Giuseppe Piccolantonio  <https://orcid.org/0000-0003-0371-9179>

REFERENCES

- Constantin G, Marconi S, Rossi B, et al. Adipose-derived mesenchymal stem cells ameliorate chronic experimental autoimmune encephalomyelitis. *Stem Cells*. 2009;27(10):2624–2635. doi:10.1002/stem.194
- Tomassini V, Matthews PM, Thompson AJ, et al. Neuroplasticity and functional recovery in multiple sclerosis. *Nat Rev Neurol*. 2012;8(11):635–646. doi:10.1038/nrneurol.2012.179
- Rocca MA, Margoni M, Battaglini M, et al. Emerging perspectives on MRI application in multiple sclerosis: moving from pathophysiology to clinical practice. *Radiology*. 2023;307(5):e221512. doi:10.1148/radiol.221512
- Barkhof F. The clinico-radiological paradox in multiple sclerosis revisited. *Curr Opin Neurol*. 2002;15(3):239–245. doi:10.1097/00019052-200206000-00003
- Pantano P. Cortical motor reorganization after a single clinical attack of multiple sclerosis. *Brain*. 2002;125(7):1607–1615. doi:10.1093/brain/awf164
- Reddy H, Narayanan S, Arnoutelis R, et al. Evidence for adaptive functional changes in the cerebral cortex with axonal injury from multiple sclerosis. *Brain*. 2000;123(11):2314–2320. doi:10.1093/brain/123.11.2314
- Biswal B, Yetkin FZ, Haughton VM, Hyde JS. Functional connectivity in the motor cortex of resting human brain using echo-planar MRI. *Magn Reson Med*. 1995;34(4):537–541. doi:10.1002/mrm.1910340409
- Jarrett C. The restless brain. *Psychologist*. 2009;22:836–839.
- Filippi M, Agosta F, Spinelli EG, Rocca MA. Imaging resting state brain function in multiple sclerosis. *J Neurol*. 2013;260(7):1709–1713. doi:10.1007/s00415-012-6695-z
- Sbardella E, Petsas N, Tona F, Pantano P. Resting-state fMRI in MS: general concepts and brief overview of its application. *Biomed Res Int*. 2015;2015:1–8. doi:10.1155/2015/212693
- Faivre A, Rico A, Zaarouf W, et al. Assessing brain connectivity at rest is clinically relevant in early multiple sclerosis. *Mult Scler*. 2012;18(9):1251–1258. doi:10.1177/1352458511435930
- Rocca MA, De Meo E, Filippi M. Functional MRI in investigating cognitive impairment in multiple sclerosis. *Acta Neurol Scand*. 2016;134(Suppl 200):39–46. doi:10.1111/ane.12654

13. Jandric D, Doshi A, Scott R, et al. A systematic review of resting-state functional MRI connectivity changes and cognitive impairment in multiple sclerosis. *Brain Connect*. 2022;12(2):112-133. doi:10.1089/brain.2021.0104
14. Tahedi M, Levine SM, Greenlee MW, Weissert R, Schwarzbach JV. Functional connectivity in multiple sclerosis: recent findings and future directions. *Front Neurol*. 2018;9:828.
15. Rossi B, Constantin G. Live imaging of immune responses in experimental models of multiple sclerosis. *Front Immunol*. 2016;7:506. doi:10.3389/fimmu.2016.00506
16. Constantinescu CS, Farooqi N, O'Brien K, Gran B. Experimental autoimmune encephalomyelitis (EAE) as a model for multiple sclerosis (MS). *Br J Pharmacol*. 2011;164(4):1079-1106. doi:10.1111/j.1476-5381.2011.01302.x
17. Tambalo S, Peruzzotti-Jametti L, Rigolio R, et al. Functional magnetic resonance imaging of rats with experimental autoimmune encephalomyelitis reveals brain cortex remodeling. *J Neurosci*. 2015;35(27):10088-10100. doi:10.1523/JNEUROSCI.0540-15.2015
18. Farinazzo A, Angiari S, Turano E, et al. Nanovesicles from adipose-derived mesenchymal stem cells inhibit T lymphocyte trafficking and ameliorate chronic experimental autoimmune encephalomyelitis. *Sci Rep*. 2018;8(1):7473. doi:10.1038/s41598-018-25676-2
19. Shah D, Deleye S, Verhoye M, Staelens S, Van der Linden A. Resting-state functional MRI and [18F]-FDG PET demonstrate differences in neuronal activity between commonly used mouse strains. *Neuroimage*. 2016;125:571-577. doi:10.1016/j.neuroimage.2015.10.073
20. Smith SM, Jenkinson M, Woolrich MW, et al. Advances in functional and structural MR image analysis and implementation as FSL. *Neuroimage*. 2004;23:S208-S219. doi:10.1016/j.neuroimage.2004.07.051
21. Bontempi P, Busato A, Bonafede R, et al. MRI reveals therapeutic efficacy of stem cells: an experimental study on the SOD1(G93A) animal model: MRI, stem cells, and the SOD1(G93A) animal model. *Magn Reson Med*. 2018;79(1):459-469. doi:10.1002/mrm.26685
22. Bontempi P, Cisterna B, Malatesta M, Nicolato E, Mucignat-Caretta C, Zancanaro C. A smaller olfactory bulb in a mouse model of Down syndrome. *Acta Neurobiol Exp*. 2020;80(4):375-380. doi:10.21307/ane-2020-034
23. Tournier JD, Smith R, Raffelt D, et al. MRtrix3: a fast, flexible and open software framework for medical image processing and visualisation. *Neuroimage*. 2019;202:116137. doi:10.1016/j.neuroimage.2019.116137
24. Andersson JLR, Skare S, Ashburner J. How to correct susceptibility distortions in spin-echo echo-planar images: application to diffusion tensor imaging. *Neuroimage*. 2003;20(2):870-888. doi:10.1016/S1053-8119(03)00336-7
25. Andersson JLR, Sotiropoulos SN. An integrated approach to correction for off-resonance effects and subject movement in diffusion MR imaging. *Neuroimage*. 2016;125:1063-1078. doi:10.1016/j.neuroimage.2015.10.019
26. Bellani M, Bontempi P, Zovetti N, et al. Resting state networks activity in euthymic bipolar disorder. *Bipolar Disord*. 2020;22(6):593-601. doi:10.1111/bdi.12900
27. Bontempi P, Podda R, Daducci A, et al. MRI characterization of rat brain aging at structural and functional level: Clues for translational applications. *Exp Gerontol*. 2021;152:111432. doi:10.1016/j.exger.2021.111432
28. Griffanti L, Salimi-Khorshidi G, Beckmann CF, et al. ICA-based artefact removal and accelerated fMRI acquisition for improved resting state network imaging. *Neuroimage*. 2014;95:232-247. doi:10.1016/j.neuroimage.2014.03.034
29. Salimi-Khorshidi G, Douaud G, Beckmann CF, Glasser MF, Griffanti L, Smith SM. Automatic denoising of functional MRI data: combining independent component analysis and hierarchical fusion of classifiers. *Neuroimage*. 2014;90:449-468. doi:10.1016/j.neuroimage.2013.11.046
30. Pamilo S, Malinen S, Hlushchuk Y, Seppä M, Tikka P, Hari R. Functional subdivision of group-ICA results of fMRI data collected during cinema viewing. *PLoS ONE*. 2012;7(7):e42000. doi:10.1371/journal.pone.0042000
31. Sforazzini F, Schwarz AJ, Galbusera A, Bifone A, Gozzi A. Distributed BOLD and CBV-weighted resting-state networks in the mouse brain. *Neuroimage*. 2014;87:403-415. doi:10.1016/j.neuroimage.2013.09.050
32. Zerbi V, Grandjean J, Rudin M, Wenderoth N. Mapping the mouse brain with rs-fMRI: an optimized pipeline for functional network identification. *Neuroimage*. 2015;123:11-21. doi:10.1016/j.neuroimage.2015.07.090
33. Grandjean J, Canella C, Anckaerts C, et al. Common functional networks in the mouse brain revealed by multi-centre resting-state fMRI analysis. *Neuroimage*. 2020;205:116278. doi:10.1016/j.neuroimage.2019.116278
34. Beckmann C, Mackay C, Filippini N, Smith S. Group comparison of resting-state FMRI data using multi-subject ICA and dual regression. *Neuroimage*. 2009;47:S148. doi:10.1016/S1053-8119(09)71511-3
35. Öngür D, Beckmann CF. Using dual regression to investigate network shape and amplitude in functional connectivity analyses. *Front Neurosci*. 2017;11:115. doi:10.3389/fnins.2017.00115
36. Seewoo BJ, Joos AC, Feindel KW. An analytical workflow for seed-based correlation and independent component analysis in interventional resting-state fMRI studies. *Neurosci Res*. 2021;165:26-37. doi:10.1016/j.neures.2020.05.006
37. Beckmann CF, Jenkinson M, Smith SM. General multilevel linear modeling for group analysis in FMRI. *Neuroimage*. 2003;20(2):1052-1063. doi:10.1016/S1053-8119(03)00435-X
38. Woolrich MW, Ripley BD, Brady M, Smith SM. Temporal autocorrelation in univariate linear modeling of FMRI data. *Neuroimage*. 2001;14(6):1370-1386. doi:10.1006/nimg.2001.0931
39. Woolrich MW, Behrens TEJ, Beckmann CF, Jenkinson M, Smith SM. Multilevel linear modelling for FMRI group analysis using Bayesian inference. *Neuroimage*. 2004;21(4):1732-1747. doi:10.1016/j.neuroimage.2003.12.023
40. Worsley KJ. Statistical analysis of activation images. In: Jezzard P, Matthews PM, Smith SM, eds. *Functional magnetic resonance imaging: an introduction to methods*. Oxford University Press; 2001. doi:10.1093/acprof:oso/9780192630711.003.0014
41. Whitesell JD, Liska A, Coletta L, et al. Regional, layer, and cell-type-specific connectivity of the mouse default mode network. *Neuron*. 2021;109(3):545-559.e8. doi:10.1016/j.neuron.2020.11.011
42. Teitelbaum D, Meshorer A, Hirshfeld T, Arnon R, Sela M. Suppression of experimental allergic encephalomyelitis by a synthetic polypeptide. *Eur J Immunol*. 1971;1(4):242-248. doi:10.1002/eji.1830010406
43. Teitelbaum D, Arnon R, Sela M. Copolymer 1: from basic research to clinical application. *Cell Mol Life Sci*. 1997;53(1):24-28. doi:10.1007/PL00000576
44. Fujino M, Funeshima N, Kitazawa Y, et al. Amelioration of experimental autoimmune encephalomyelitis in Lewis rats by FTY720 treatment. *J Pharmacol Exp Ther*. 2003;305(1):70-77. doi:10.1124/jpet.102.045658
45. Steinman L, Patarca R, Haseltine W. Experimental encephalomyelitis at age 90, still relevant and elucidating how viruses trigger disease. *J Exp Med*. 2023;220(2):e20221322. doi:10.1084/jem.20221322

46. Blankenhorn EP, Butterfield R, Case LK, et al. Genetics of experimental allergic encephalomyelitis supports the role of T helper cells in multiple sclerosis pathogenesis. *Ann Neurol*. 2011;70(6):887-896. doi:10.1002/ana.22642
47. Bearoff F, Case LK, Kremntsov DN, et al. Identification of genetic determinants of the sexual dimorphism in CNS autoimmunity. *PLoS ONE*. 2015; 10(2):e0117993. doi:10.1371/journal.pone.0117993
48. Bannerman PG, Hahn A, Ramirez S, et al. Motor neuron pathology in experimental autoimmune encephalomyelitis: studies in THY1-YFP transgenic mice. *Brain*. 2005;128(8):1877-1886. doi:10.1093/brain/awh550
49. Hamilton AM, Forkert ND, Yang R, et al. Central nervous system targeted autoimmunity causes regional atrophy: a 9.4T MRI study of the EAE mouse model of multiple sclerosis. *Sci Rep*. 2019;9(1):8488. doi:10.1038/s41598-019-44682-6
50. Parmar K, Stadelmann C, Rocca MA, et al. The role of the cerebellum in multiple sclerosis—150 years after Charcot. *Neurosci Biobehav Rev*. 2018;89: 85-98. doi:10.1016/j.neubiorev.2018.02.012
51. Sbardella E, Upadhyay N, Tona F, et al. Dentate nucleus connectivity in adult patients with multiple sclerosis: functional changes at rest and correlation with clinical features. *Mult Scler*. 2017;23(4):546-555. doi:10.1177/1352458516657438
52. Cocozza S, Pontillo G, Russo C, et al. Cerebellum and cognition in progressive MS patients: functional changes beyond atrophy? *J Neurol*. 2018; 265(10):2260-2266. doi:10.1007/s00415-018-8985-6
53. Pasqua G, Tommasin S, Bharti K, et al. Resting-state functional connectivity of anterior and posterior cerebellar lobes is altered in multiple sclerosis. *Mult Scler*. 2021;27(4):539-548. doi:10.1177/1352458520922770
54. Tommasin S, Iakovleva V, Rocca MA, et al. Relation of sensorimotor and cognitive cerebellum functional connectivity with brain structural damage in patients with multiple sclerosis and no disability. *Eur J Neurol*. 2022;29(7):2036-2046. doi:10.1111/ene.15329
55. Roosendaal SD, Schoonheim MM, Hulst HE, et al. Resting state networks change in clinically isolated syndrome. *Brain*. 2010;133(6):1612-1621. doi: 10.1093/brain/awq058
56. Vercellino M, Masera S, Lorenzatti M, et al. Demyelination, inflammation, and neurodegeneration in multiple sclerosis deep gray matter. *J Neuropathol*. 2009;68(5):489-502. doi:10.1097/NEN.0b013e3181a19a5a
57. d'Ambrosio A, Hidalgo de la Cruz M, Valsasina P, et al. Structural connectivity-defined thalamic subregions have different functional connectivity abnormalities in multiple sclerosis patients: implications for clinical correlations. *Hum Brain Mapp*. 2017;38(12):6005-6018. doi:10.1002/hbm.23805
58. Schoonheim MM, Geurts JGG, Wiebenga OT, et al. Changes in functional network centrality underlie cognitive dysfunction and physical disability in multiple sclerosis. *Mult Scler*. 2014;20(8):1058-1065. doi:10.1177/1352458513516892
59. Tona F, Petsas N, Sbardella E, et al. Multiple sclerosis: altered thalamic resting-state functional connectivity and its effect on cognitive function. *Radiology*. 2014;271(3):814-821. doi:10.1148/radiol.14131688
60. Hidalgo de la Cruz M, d'Ambrosio A, Valsasina P, et al. Abnormal functional connectivity of thalamic sub-regions contributes to fatigue in multiple sclerosis. *Mult Scler*. 2018;24(9):1183-1195. doi:10.1177/1352458517717807
61. Sbardella E, Tona F, Petsas N, Pantano P. DTI measurements in multiple sclerosis: evaluation of brain damage and clinical implications. *Mult Scler Int*. 2013;2013:1-11. doi:10.1155/2013/671730
62. Wang X, Cusick MF, Wang Y, et al. Diffusion basis spectrum imaging detects and distinguishes coexisting subclinical inflammation, demyelination and axonal injury in experimental autoimmune encephalomyelitis mice. *NMR Biomed*. 2014;27(7):843-852. doi:10.1002/nbm.3129
63. Budde MD, Xie M, Cross AH, Song SK. Axial diffusivity is the primary correlate of axonal injury in the experimental autoimmune encephalomyelitis spinal cord: a quantitative pixelwise analysis. *J Neurosci*. 2009;29(9):2805-2813. doi:10.1523/JNEUROSCI.4605-08.2009
64. Nishioka C, Liang HF, Barsamian B, Sun SW. Sequential phases of RGC axonal and somatic injury in EAE mice examined using DTI and OCT. *Mult Scler Relat Disord*. 2019;27:315-323. doi:10.1016/j.msard.2018.11.010
65. Lenzi D, Conte A, Mainero C, et al. Effect of corpus callosum damage on ipsilateral motor activation in patients with multiple sclerosis: a functional and anatomical study. *Hum Brain Mapp*. 2007;28(7):636-644. doi:10.1002/hbm.20305
66. Smith PA, Schmid C, Zurbrugg S, et al. Fingolimod inhibits brain atrophy and promotes brain-derived neurotrophic factor in an animal model of multiple sclerosis. *J Neuroimmunol*. 2018;318:103-113. doi:10.1016/j.jneuroim.2018.02.016
67. MacKenzie-Graham A, Tinsley MR, Shah KP, et al. Cerebellar cortical atrophy in experimental autoimmune encephalomyelitis. *Neuroimage*. 2006; 32(3):1016-1023. doi:10.1016/j.neuroimage.2006.05.006
68. Pol S, Liang S, Schweser F, et al. Subcutaneous anti-CD20 antibody treatment delays gray matter atrophy in human myelin oligodendrocyte glycoprotein-induced EAE mice. *Exp Neurol*. 2021;335:113488. doi:10.1016/j.expneurol.2020.113488

SUPPORTING INFORMATION

Additional supporting information can be found online in the Supporting Information section at the end of this article.

How to cite this article: Bontempi P, Piccolantonio G, Busato A, et al. Resting-state functional magnetic resonance imaging reveals functional connectivity alteration in the experimental autoimmune encephalomyelitis model of multiple sclerosis. *NMR in Biomedicine*. 2024;37(6):e5127. doi:10.1002/nbm.5127